Using predictive models unravel the potential of titanium oxide loaded activated carbon for removal of leachate ammoniacal nitrogen

Kulbir Singh
Department of Civil Engineering, Maharishi Markandeshwar (Deemed to be University), Mullana, Ambala - Pin code - 133207, (Haryana), India
Rajesh Kumar Lohchab
rajeshlohchab@gmail.com
Department of Environmental Science & Engineering, Guru Jambheshwar University of Science and Technology, Hisar - Pin Code- 125001, (Haryana), India
Vikas Beniwal
Department of Microbiology, Central University of Haryana, Mahendergarh, Pin code - 123031, (Haryana), India
Chadetrik Rout
Department of Civil Engineering, Maharishi Markandeshwar (Deemed to be University), Mullana, Ambala - Pin code - 133207, (Haryana), India

Research Article

Keywords: Leachate, Almond Shell, TiO2 nanoparticle, Phonon mode, Adsorption, Ammonia Nitrogen

Posted Date: June 1st, 2023

DOI: https://doi.org/10.21203/rs.3.rs-2969310/v1

Additional Declarations: No competing interests reported.

Version of Record: A version of this preprint was published at Environmental Monitoring and Assessment on May 16th, 2024. See the published version at https://doi.org/10.1007/s10661-024-12689-w.

Abstract

The TiO_2 nanocomposite efficiency was determined under optimized conditions with activated carbon to remove ammoniacal nitrogen (NH_3-N) from the leachate sample. In this work, the facile impregnation and pyrolysis synthesis method was employed to prepare the nanocomposite, and their formation was confirmed using the XRD and Raman studies. In contrast, Raman phonon mode intensity ratio I_D/I_G increases from 2.094 to 2.311, indicating the increase of electronic conductivity and defects with the loading of TiO_2 nanoparticles. The optimal conditions for achieving maximum NH_3-N removal of 75.8% were found to be a pH of 7, a dose of 1.75 mg/L, and a temperature of 30^oC, with a corresponding time of 160 minutes. All adsorption isotherm records were properly fitted, and linear plots were utilized to analyze NH_3-N removal through adsorption kinetic models. Additionally, an effective central composite design (CCD) of response surface methodology (RSM) was employed to investigate the efficient removal of NH_3-N.

Highlights

1) TiO_2 nanoparticles loaded on activated carbon was prepared.

2) Raman phonon mode intensity ratio ID/IG increased from 2.094 to 2.311 of adsorbent.

3) At optimum conditions NH_3-N removal was found to be of 75.8%.

4) RSM results shows the performance of adsorption process.

1. Introduction

The primary method used worldwide to dispose of industrial and municipal solid waste is through landfilling. However, this method generates significant quantities of heavily contaminated leachate that require proper collection and treatment. Landfill leachate can interfere with the processes involved in treating wastewater due to its high levels of ammonia and resistant organic compounds (Yang et al., 2023). The high concentration of ammoniacal nitrogen in leachate has been a persistent issue faced by landfill operators for decades. Leachate has high ammoniacal nitrogen concentrations over long periods due to the slow leaching of nitrogen-producing wastes and no significant transformation mechanism for NH_3-N in landfills (Haslina et al., 2021). A survey of the literature revealed that leachate generated from landfill sites contains numerous toxic elements represented by predictable metals and enriched with nitrogen and other complex organic compounds (Detho et al., 2021; Gripa et al., 2023; Naji et al., 2020; Singh, 2021). The content of biodegradable and non-biodegradable constituents in leachate is generally so elevated that a very small volume may contaminate a significant amount of groundwater (Shadi et al., 2020; Singh et al., 2021). As a result, the treatment of leachate has become a major concern for waste management. Currently, various methods are employed in an integrated manner to purify leachate in the leachate treatment chain (De Almeida et al., 2022; Song et al., 2022). Typically, primary and/or secondary

technologies are utilized to treat landfill leachate, but further purification is necessary due to the presence of heavy macro and micro-contaminants (Song et al., 2022). Biological methods/techniques are better suited to treat freshly generated leachate and are ineffective in aged/stabilized leachate (Z. Li et al., 2018). Because of the high concentrations of ammoniacal nitrogen in leachate deposits, direct biological treatment resulted its low elimination. Simultaneously, the bio-recalcitrant organic matter must be removed using physico-chemical methods for biologically treated effluent. Hence, physico-chemical treatment has become more attractive in the treatment of landfill leachate. However, various authors have reported the application of multiple adsorbents to remove ammoniacal nitrogen, and there is an increasing interest in using cheap, commercially available ammoniacal nitrogen adsorption materials (Aziz et al., 2004; Huong et al., 2019; Singh et al., 2018). Furthermore, the preparation of activated carbon made from almond shells has previously been recognized in substantial research (Ahsaine et al., 2018; Saka et al., 2023). Moreover, adding metal oxide to activated carbon has numerous advantages such as enhance thermal constancy, increase active sorption sites, and improve adsorbent yield (Ghaedi et al., 2013; Liu et al., 2020; Pipil et al., 2022; Rodriguez-Narvaez et al., 2019). Saka et al. (2023) utilized microwave heating and KOH chemical process to prepare Sulphur-doped activated carbon prepared from almond shells, and found that it exhibited a remarkable adsorption capacity of 282.70 mg/g for Cd (II) adsorption. Therefore, in the present investigation an economical & efficient adsorbent, from waste almond shell-activated carbon incorporated with TiO_2 nanoparticles, was synthesized and subsequently characterized. Under optimised conditions, the effectiveness of TiO_2@ASAc for the elimination of NH_3-N from the leachate sample was estimated. To get conclusive concepts on NH_3-N removal from leachate *via* adsorption techniques, thermodynamics studies, kinetics, equilibrium isotherms, and RSM were used and explored.

2. Materials and methods

2.1. *Characterisation of materials*

The moisture, volatile, and ash content of RAS were determined as mentioned in ASTM standard methods. An elemental analyser was used to determine the extent of H, C, S, and N. It was perceived that high carbon (49.91%), high volatile (77.59%), and little ash content made it further acceptable for the synthesis of activated carbon. Required volume of leachate sample was produced from Municipal solid waste (MSW) in an anaerobic digester/bioreactor and after stabilization it characterized for further treatment (Table 1).

Table 1
Physico-chemical properties of stabilised leachate

Parameter	Value	Parameter	Value
pH	6.2 ± 0.21	Na^+	312 ± 2.3
EC (mS cm^{-1})	16 ± 0.91	PO_4^{3-}	65 ± 0.9
Turbidity	63 ± 2	Ca^{2+}	652 ± 1.7
COD	9250 ± 158	Mg^{2+}	190 ± 2.8
BOD	2420 ± 40	SO_4^{2-}	150 ± 1.1
BOD_5/COD	0.26	Cl^-	940 ± 18
Total alkalinity	3200 ± 34	Fe^{2+}	25 ± 1.1
TDS	9321 ± 172	Zn	3.47 ± 0.2
Suspended solids	398 ± 12	Cr	0.98 ± 0.09
Volatile solid	304 ± 5	Ni	0.34 ± 0.04
Fixed solid	94 ± 3	Cd	0.79 ± 0.09
TKN	980 ± 14	Cu	0.39 ± 0.03
NH_3-N	735 ± 9	Pb	0.99 ± 0.08
K^+	261 ± 2.1	Co	0.58 ± 0.07

2.2. Preparation of TiO_2 loaded on ASAc

The almond shell was finely grounded, sieved, and placed in a tube furnace under the nitrogen flow. Thereafter, carbonized almond shell (CAS) was soak with $ZnCl_2$ at a ratios of 1:3. Pyrolysis was carried out in the N_2 flow tubular furnace at 800°C for about 90 minutes (Taha et al., 2018). Following the synthesis of ASAc, TiO_2 nanoparticles were impregnated on the capable ASAc in a 2:1 ratio (Hosseini et al., 2007).

2.3. *Characterization of TiO_2 loaded almond shell adsorbent*

To characterize TiO_2@ASAc, several analytical techniques were employed, including X-ray diffraction (XRD), Raman spectroscopy, and Brunauer–Emmett–Teller (BET) analysis. The BET surface area analysis of ASAc and TiO_2@ASAc was conducted using BET Quantachrome Instruments, and N_2 adsorption-desorption isotherms were used to determine the specific surface area and pore volume. Powder XRD data were collected using a Rigaku Miniflex-II diffractometer with Cu Kα radiation (λ =

1.5418 A^{o}) in the 2theta range of 10^{o} to 80^{o} at a scanning rate of 2^{o}/min. Raman scattering measurements were performed using a Renishaw micro-Raman system equipped with a Peltier cooled CCD detector and 514.5 nm excitation laser.

2.4. *Batch adsorption*

Batch mode experiments were conducted to observe the NH3-N removal percentage under varying conditions, including pH levels ranging from 2 to 10, contact time from 20 to 200 minutes, dose from 5 to 50 g/L, and temperature between 25℃ to 40℃. The various isotherm models were used to implement nonlinear equations in monolayer and multilayer adsorption techniques. For this well proven isotherms models i.e., Redlich-Peterson, Freundlich, Koble-Corrigan, Hill, Khan, Toth etc. are used (Supplementary Table 1). The linear plots were used to analyse NH_3-N removal using adsorption kinetic models of pseudo first & second order, as well as intraparticle diffusion (Supplementary Table 2). The inter-relationship between input and output parameters for effective removal of NH_3-N by TiO_2@ASAc was investigated using CCD of surface response methodology. Based on experimental studies, four independent variables were considered: (i) pH (2.0–10.0), (ii) dose (0.25–2.50 g/50L), (iii) contact time (20–200 min.), and temperature (25–40℃). Thirty sets of experiments were developed using CCD of Design-Expert software 13 for removal of NH_3-N. For each independent variable, five levels (-1, 0, + 1, -α, +α) were used. To describe the relationship between independent variables and their detected responses, a quadratic polynomial equation was used (Bezerra et al., 2008). ANOVA, model graphs (actual *vs* predicted plots), 3D-Plots as well as contour plots were used to investigate the NH_3-N removal by TiO_2@ASAc.

2.5. *Reusability study*

Adsorbents with nanoparticles were re-collected and used again in our investigation i.e., for adsorption process. One gram of adsorbent material was washed with variable concentrations of HCl i.e., 0.05, 0.1, and 0.15 M and shaken in a shaker up to 3 hours at 150 rpm. The filtered adsorbents were thoroughly washed with deionized water and then dried for 24 h in an oven at 80℃. All the adsorbents were reused for NH_3-N removal up to a maximum of three times.

3. Results and Discussions

3.1. Characterization of the ASAc

The N_2 adsorption-desorption isotherm was used to determine the porous structure of activated almond shell filled with TiO_2, as shown in Fig. 1(a). All the samples show classic IV isotherm with the irreversible domain, and curves represent the type H3 hysteresis, suggesting that the materials' non-rigid masses form slit-shaped pores. TiO_2@ASAc had a nearly threefold greater BJH-specific surface area (153.3 m^2/g) than structured ASAc (54.7 m^2/g), and the total porosity increased from 0.038 to 0.135 cm^3/g.

Activated almond shells & TiO_2-loaded activated almond shells had average pore sizes of 2.91 & 3.47 nm, respectively.

The crystal structure of all the samples (1AS, 2AS, 3AS, and 4AS) were analysed by XRD. The XRD pattern of the 1AS sample, as illustrated in Fig. 1(b), shows three peaks near 15.8, 22.12, and 34.67 ^{o}, indicating cellulose I type crystals. However, the XRD spectrum of 2AS indicating the existence of cellulose and carbonaceous crystalline structure (strong diffraction peaks at 16.64, 22.19, 25.98, 29.58, 34.67, and 43.56^{o}). Because the formation of crystalline phases is initiated by thermal treatment, which generates thermal kinetic energy (Kumar & Jena, 2015). Following the loading of TiO_2, the XRD patterns of the 3AS and 4AS samples displayed intense diffraction peaks at 25.31, 37.83, 48.07, 54.57, and 62.75^{o}, which corresponded to the anatase phase. Additionally, strong diffraction peaks at 27.47 and 36.11º, corresponding to the rutile phase, were observed, along with diffraction planes 101, 103, 200, 105, and 213. Furthermore, certain sequences also express some less intensity peaks, confirming the existence of activated carbon and these observations are more consistent with other findings (Bel Hadjltaief et al., 2015; X. Li et al., 2018).

Figure 1(c) shows the Raman spectra of selected samples. For 2AS sample, the spectra show three peaks at 1337.4, 1592.3, and a broad peak in the range 2250–3200 cm^{-1} attributed to (CH_2) wagging bond (called D band), (OH) bending in the carbon samples (G band) and a combination of 2D and D + G bands. For the 1AS sample, no characteristic Raman spectra are observed due to the low incident laser power. The 3AS sample, spectra shows the signature of both TiO_2 and carbon phases. The low intensity of phonon modes of TiO_2 anatase phase compared to carbon phase indicates activated carbon in high amounts. For the TiO_2 phase, the phonon modes were observed at 150.2, 202.1, 388.9, and 504.7 cm^{-1}. The intensity ratio of the D and G bands, expressed as I_D/I_G, used to calculate structural disorder and electronic conductivity. The ratio increases from 2.094 to 2.311 (in the case of TiO_2@ASAc) indicates the increase of electronic conductivity and defects with the loading of TiO_2 nanoparticles. Our results are in agreement with previous finding of Omri and Benzina, 2019.

3.2. NH_3-N removal experiment

With variable pH, temperature levels, dose, and contact time, the percentage of NH_3-N removal of leachate was investigated. During the optimization process, one parameter's value varied while the remaining factors remained constant.

3.2.1. Influence of pH on NH_3-N removal

pH is considered as one of the most critical and influencing factor which significantly affects the adsorbent's surface charge and degree of ionization (Wu et al., 2012). Experiments were carried out with pH ranging from 2 to 10, while other variables were held constant i.e., adsorbent dose at 30.0 g/L, temperature at 30.0 ± 1℃, and NH_3-N concentration at 735 mg/L. The percentage of NH_3-N removed

increased with increase in pH and observed maximum at pH 7 (Fig. 2(a)). However, beyond pH 7 resulted in a decrease in NH_3-N removal and is supported by literature (Hu et al., 2016). The ammonium ions were neutralised and converted to ammonia by hydroxyl ions (OH^-) at higher pH. Therefore, it is quite difficult to remove this form of ammonia using adsorbents, and TiO_2@ASAc capability is also decrease at higher pH values (Ferraz & Yuan, 2020; Mosanefi et al., 2021). As a result, pH 7.0 was determined to be the optimum pH for conducting other experiments.

3.2.2. Dose effect on NH_3-N reduction

Figure 2(b) shows that the percent removal of NH_3-N increased from 22.9 to 81.5, with the increasing concentration of TiO_2@ASAc (0.25 to 2.5 g/50 mL). It can be seen as increased availability of binding sites/surface area with increasing adsorbent dose (Hashemian et al., 2014). Beyond 1.75 g/50 mL, there was no expressive effect on NH_3-N removal. Tamilselvi and Radha (2017) reported similar observations during wastewater treatment. Furthermore, adsorbent adsorption capacities for NH_3-N showed a reverse trend to removal efficiency and was found to be decreased from 33.66 to 11.98 mg/g with an increasing biosorbent dosage. This could be due to accumulation of substantial amount of absorbent dose, which minimise the net surface area of the biosorbent (Alorabi et al., 2020). Therefore, an optimal dose of TiO_2@ASAc was found to be 1.75 g/50 mL, resulting in 75.8% removal efficiency of NH_3-N.

3.2.3. Influence of contact time on NH_3-N removal

To study the effect of contact time on NH_3-N removal, contact time was varied from 20 to 200 minutes and other variables were kept constant i.e., at pH 7.0, dose 1.75 g, temperature 30.0 ± 1°C, and 735 mg/L of NH_3-N of leachate (Fig. 2(c)). In the first 20 minutes, the TiO_2@ASAc adsorbent removed 42.9% of NH_3-N (an adsorption capacity of 9.01 mg/g). When the contact time was extended to 160 minutes, there was a corresponding increase in NH_3-N removal, with a removal efficiency of 75.8% and a sorption capacity of 15.92 mg/g. Further increase in the contact time shows insignificant shifts in NH_3-N removal. Initially, this could be attributed to availability of more surface-active sites on the adsorbent, which increased the sorption rate. However, as contact time was increased, sorption decreased due to the pollutants filling active sites, and the adsorbent reached equilibrium (Faisal et al., 2020).

3.2.4. Influence of temperature on NH_3-N removal

For sorption process temperature plays a vital role and the influence of temperature on NH_3-N removal were observed by varying the temperature from 25 to 40°C (Fig. 1(d)). With increasing temperature, the NH_3-N removal increased from 68.2 to 81.5%, indicating an endothermic process. Due to increase in temperature, adsorbate diffusion increased across the surface layer, as did intraparticle dispersal within the adsorbate pores (Peng et al., 2012). At a temperature of 30°C, the NH_3-N removal efficiency was found to be at its maximum, reaching 75.8% with a sorption capacity of 15.92 mg/g. Further increases in temperature did not result in significant differences in NH_3-N uptake, leading to the selection of 30°C as the optimal temperature.

3.3. Isotherms of Adsorption

Adsorption isotherms of NH_3-N reduction by TiO_2@ASAc were implemented using nonlinear forms at different adsorbent doses (0.25 to 2.5 g/50 mL). Figure 3 shows the q_e vs. C_e relationships. The Hill isotherm model, with a binding interaction of 0.6749, described the combined phenomenon of NH_3-N species binding to TiO_2@ASAc. The Khan isotherm was established for diverse adsorption processes, with A_k values of 0.3261 for NH_3-N adsorption that were not equal to 1.0, and final concentration (C_e) values that were higher (as shown in Table 2). This suggests that the model was transformed to the Freundlich isotherm. The Redlich-Peterson model adheres to Henry's law, displaying the Langmuir model at low concentrations and the Freundlich model at higher concentrations (where b_R is close to zero). Since the calculated value of b_R (0.3) was close to zero, the Freundlich model is followed. The model of Toth isotherm explains heterogeneous adsorption across a Quasi-Gaussian energy unsymmetrical distribution at low and high concentrations. For NH_3-N adsorption, the Toth isotherm constant “t” was calculated as 3.02. The Koble-Corrigan isotherm, which combines the Langmuir and Freundlich isotherms, is commonly used for heterogeneous adsorption processes. Calculated value of D was found to be 0.4085, which is < 1.000. As a result, the Koble-Corrigan model was unable to describe investigated data. The Freundlich isotherm was observed to be suitable based on the nonlinear model values, with R^2 (0.9847) and 1/n (1.4817), as shown in Table 2. These models were applied to demonstrate the ability of TiO2@ASAc to effectively reduce NH3-N through diverse layer adsorption.

Table 2
Values of different nonlinear adsorption isotherm parameter

Isotherms	Parameter	Value
Freundlich	K_f	0.000453
	n	1.48178
	R^2	0.9847
Hill	Q_h	3842.21
	K_d	8.479E6
	n_h	0.67491
	R^2	0.9847
Khan	Q_k	0.000413
	B_k	1.159
	A_k	0.32611
	R^2	0.9847
Redlich–Peterson	K_R	0.21408
	a_R	471.922
	b_R	0.32523
	R^2	0.9847
Toth	K_t	0.000470
	a_t	4.872
	t	3.02421
	R^2	0.9846
Koble-Corrigan	A	0.00125
	B	-0.003761
	D	0.40852
	R^2	0.9874

3.4. Adsorption kinetic studies

The research investigated the rate controlling steps of NH_3-N reduction adsorption using TiO_2@ASAc through pseudo first and second-order kinetics and intraparticle diffusion. In Fig. 4(a), a linear plot of log (q_e-q_t) against t was used in pseudo first-order kinetics to determine the slope (K_1) and intercept (log q_e). However, Table 3 showed that the sorption capacity (q_e) calculated from the linear plot did not match the experimental results, indicating that the order rate expression was not applicable to NH_3-N removal. On the other hand, Fig. 4(b) presented the plotting (t/q_t vs t) of pseudo-second-order kinetics, which provided values for q_e and K_2 through the slope and intercept. In case of pseudo-second-order, the findings shows that the q_e value (18.51 mg/g) was observed to be more significant than the experimental value (16.15 mg/g). For NH_3-N reduction, the R^2 (0.997) was established to be more significant and more importantly follows pseudo-second-order kinetics. Similar findings have been reported by (Singh et al., 2021, 2022). The intra-particle diffusion rate plots q_t *vs* $t^{1/2}$ provide rate constant of intra-particle diffusion (K_{id}), and the thickness of the boundary layer is represented by the intercept (C) (Fig. 4(c)). If the plot does not traverse through the origin, it is only the rate regulating step. The correlation coefficient (R^2) value of 0.943 indicates that the intra-particle diffusion is insignificant for current studies.

Table 3
Parameter study of kinetic models for NH_3-N sorption

Model	Parameter	Value
Pseudo-first order	K_1 (min^{-1})	0.018
	q_e (mg/g)	9.90
	R^2	0.77
Pseudo-second order	K_2 (g /mg min^{-1})	0.00205
	q_e (mg/g)	18.51
	R^2	0.99
Intraparticle diffusion	K_{id} (mg g^{-1} $min^{-1/2}$)	0.77
	C	6.15
	R^2	0.94
Experimental value	q_e(mg/g)	16.15

3.5. Thermodynamic investigation

Thermodynamic studies of NH_3-N removal at various temperatures (i.e., 298K, 303K, 308K, and 313K) were carried out to determine the thermal actions of the sorption activity. Changes in thermodynamic

factors such as Gibb's free energy (ΔG⁰), entropy (ΔS⁰) and enthalpy (ΔH⁰) were calculated using the following equation to reveal reaction spontaneity.

$$lnK_d = \frac{\Delta S}{R} - \frac{\Delta H}{RT} (1)\ \Delta G^0 = \Delta H^0 - T\Delta S^0\ (2)\ K_d = \frac{C_a}{C_e} (3)$$

The linear plot slope and intercept between lnK_d *vs* 1/T were used to calculate the values of ΔH° and ΔS°. The presence of negative ΔG⁰ values indicated that the removal of NH_3-N by TiO_2@ASAc was spontaneous, and the decrease in its values as temperature increased replicated that high temperatures were favourable for adsorption (Table 4). The positive enthalpy change value (ΔH°=35.80 kJmol^{-1}) demonstrated that the NH_3-N sorption interface with TiO_2@ASAc was endothermic, and their adsorption equilibrium increased as temperature increased. Positive entropy change value (ΔS⁰= 126.90 J/mol/K) indicated certain structural modifications and more adsorbent solution interface randomness.

Table 4
Temperature-dependent thermodynamic parameters for NH_3-N sorption

Temperature (K)	ΔG⁰(*KJ/mol*)	ΔH° (*KJ/mol*)	ΔS⁰ (*J/molK*)
298	-2.0069		
303	-2.6414	35.8	126.904
308	-3.2759		
313	-3.9104		

3.6. RSM-CCD Analysis

The experimental design utilized was RSM-CCD which included six replications at the center point for each independent variable factor, namely pH, dose, contact time, and temperature, as outlined in Table 5. The quadratic Eq. (4) expresses the correlation between variable factors and responses, which were best suited for variable relationships and suitable for predicting NH_3-N sorption.

Table 5
RSM-CCD independent variables

Factors	Lower Limit (-1)	Centre (0)	Upper Limit (+ 1)	-alpha (-α)	alpha (α)
A: pH	4	6.5	9	1	1
B: Dose	1.25	1.75	2.25	1	1
C: Time	100	150	200	1	1
D: Temperature	25	32.50	40	1	1

NH_3-N (%) removal Y_{pred}= +73.28 + 3.78 A + 4.74 B + 1.64 C + 1.23 D + 2.58 AB + 1.03 AC – 1.04 AD + 0.0037 BC – 0.0638 BD – 0.8337 CD – 10.29 A^2 – 8.36 B^2 – 4.46 C^2 – 3.61 D^2 (4)

The mutual effect of variable factors in contour plots and 3-D response is represented in Fig. 5(b-d). These demonstrate NH_3-N reduction as adsorbent dose and pH were increased. When the pH increased from 4 to 6.5, the NH_3-N sorption increased, thereafter it decreases as the pH increases, indicating the inhibiting impact of high pH. The efficiency of NH_3-N removal was improved by increasing the dose from 1.25g to 1.75g; however, there was no significance difference thereafter. The percentage of NH_3-N removal improve with increasing temperature and time and; the interactive effect of pH is express in Fig. 5(e-g). The maximum NH_3-N removal was 73.28% at optimum pH 6.5, dose 1.75 g, contact time 2.5hrs, temperature 32.5°C, and represented in 3D plots. The observed optima result for NH_3-N removal employing TiO_2@ASAc adsorbent, evaluated by the RSM-CCD algorithm model was promising.

According to Table 6, the analysis of variance (ANOVA) indicates that the model is best fitted for NH_3-N removal, with $p < 0.0001$ and F-286.92. The adequate precision value of 58.747, which is greater than 4, confirms the authenticity and suitability of the model. The infallibility of the experimental data is also confirmed by a CV of 2.26%. The adjusted R^2 of 0.993 and predicted R^2 of 0.980 (NH_3-N removal) indicate that the experimental design was well-suited to the model, as depicted in Fig. 5(a).

Table 6
ANOVA for NH_3-N removal percentage * SS: Sum of Squares, DF: Degree of freedom, MS: Mean Square

Source	SS	DF	MS	F-value	p-value	
Model	5528.91	14	394.92	286.92	< 0.0001	significant
A	343.83	1	343.83	249.80	< 0.0001	
B	538.84	1	538.84	391.48	< 0.0001	
C	64.94	1	64.94	47.18	< 0.0001	
D	36.26	1	36.26	26.34	0.0001	
AB	106.30	1	106.30	77.23	< 0.0001	
AC	16.97	1	16.97	12.33	0.0031	
AD	17.22	1	17.22	12.51	0.0030	
BC	0.0002	1	0.0002	0.0002	0.9900	
BD	0.0650	1	0.0650	0.0472	0.8309	
CD	11.12	1	11.12	8.08	0.0123	
A^2	2905.07	1	2905.07	2110.57	< 0.0001	
B^2	1915.92	1	1915.92	1391.94	< 0.0001	
C^2	545.04	1	545.04	395.98	< 0.0001	
D^2	357.74	1	357.74	259.90	< 0.0001	
Residual	20.65	15	1.38			
Lack of Fit	18.23	10	1.82	3.78	0.0776	Not significant
Pure Error	2.41	5	0.4825			
Cor Total	5549.56	29				

* SS: Sum of Squares, DF: Degree of freedom, MS: Mean Square

The mutual effect of the variable factors on NH_3-N reduction is illustrated in contour plots and 3-D response plots in Fig. 5(b-d). The results show that increasing the adsorbent dose and pH led to an increase in NH_3-N sorption. However, as the pH increased beyond 6.5, NH_3-N sorption decreased, indicating the inhibiting effect of high pH. Along it, increasing the dose from 1.25g to 1.75g improved the efficiency of NH_3-N removal, but there was no significant difference thereafter. The percentage of NH_3-N removal improved with increasing temperature and time, and; the interactive effect of pH is expressed in Fig. 5(e-g). The maximum NH_3-N removal of 73.28% was achieved at the optimum conditions of pH 6.5,

dose 1.75 g, contact time 2.5 hrs, and temperature 32.5°C, as shown in the 3D plots. The observed optimum result for NH_3-N removal using the TiO_2@ASAc adsorbent, evaluated by the RSM-CCD algorithm model, is promising.

3.7 Regeneration effectiveness of TiO_2@ASAc

The efficiency of regeneration is important for economic and environmentally friendly wastewater treatment technologies. Therefore, a good adsorbent should have better adsorption efficiency, which should be important in regeneration and recycling practices. The NH_3-N removal efficiency of the sorbent increased as the hydrochloric acid concentration increased from 0.05M to 0. 15M (Fig. 9). At 0.15 M HCl, the removal efficiencies were calculated to be 69.2, 58.5, and 53.4% at Cycles 1, 2, and 3 respectively. As the number of cycles increases the NH_3-N removal percentage decreases as shown in Fig. 6. Thamilselvi & Radha (2017) conducted a similar investigation with the silver nanoparticles loaded corncob. In the 3rd regeneration cycle of adsorbent, more than 50% NH_3-N was removed which revealed the cost effectiveness and prominent characteristics of synthesized TiO_2@ASAc.

Conclusion

An agro-waste precursor, the almond shell, was synthesized into activated carbon through physical and chemical activation practices. XRD and Raman's study confirms the formation of both the carbon and TiO_2 phases. The ratio of the D and G bands shows enhancement in electronic conductivity with TiO_2 loading. The best removal efficiency of NH_3-N 75.8% with an adsorption efficiency of 15.92 mg/g was found at optimal conditions. All the nonlinear isotherm models well fitted to the observed results having R^2 values of 0.9847, 0.9847, 0.9847, 0.9847, 0.9846, and 0.9874, respectively, indicating multilayer sorption behavior. During pseudo-second-order kinetics, the calculated value of adsorption capacity 18.51mg/g was found nearly equal to the observed value 16.15 mg/g along with a high R^2 value of 0.997 that express adsorption process adapted pseudo-second-order model. The adsorption process demonstrates spontaneous and endothermic behavior in accordance with thermodynamics. The strong correlation coefficients between adjusted R^2 (0.9928) and predicted R^2 (0.9804) suggest that the surface response methodology aligns well with the CCD model. The experimental data is consistent with the design experiment, which determined the optimal values for pH (6.5), dose (1.75), contact time (150 minutes), and temperature (32.5℃). The regenerated sorbent exhibited valid efficiency for up to three cycles. In conclusion, the study concludes that TiO_2@ASAc is a cost-effective adsorbent that is effective in leachate treatment.

Declarations

Acknowledgement: The authors acknowledge the TEQIP-III GJUS&T, Hisar for providing financial assistance with letter number TEQIP-III/2018/1841-114.

Author contribution All authors contributed to the study conception and design. Material preparation, data collection, and analysis were performed by Kulbir Singh and Chadetrik Rout. The first draft of the manuscript was written by Rajesh Kumar Lohchab and Vikas Beniwal. All author commented on the previous versions of the manuscript and all authors read and approved the final manuscript.

Funding This work was supported by a Technical Education Quality Improvement Programme of Government of India (TEQIP) ID TEQIP-III/2018/1841-114. The grant is funded by the World Bank Programme under an assisted project designed to improve the quality of technical education.

Availability of data and materials The manuscript included the all data investigated during the study and authors have read, understood, and have fulfilled as applicable with the statement on "Ethical responsibilities of Authors". Also, no changes can be made to authorship once the paper is submitted.

Declaration on conflict of interest: There is no conflict of interest between authors and organizations.

Ethical approval: This article does not contain any studies with human participants or animals performed by any of the authors.

References

1. Abdulla, F. H. (2014). Removal of Chromium (III) Ions from its Aqueous Solution on Adsorbent Surfaces: Charcoal, Attapulgite and Date Palm Leaflet Powder. *Iraqi Journal of Science*, *55*(4A), 1415–1430.
2. Ahsaine, H. A., Zbair, M., Anfar, Z., Naciri, Y., El Alem, N., & Ezahri, M. (2018). Cationic dyes adsorption onto high surface area 'almond shell'activated carbon: Kinetics, equilibrium isotherms and surface statistical modeling. *Materials Today Chemistry*, *8*, 121–132.
3. Alorabi, A. Q., Alharthi, F. A., Azizi, M., Al-Zaqri, N., El-Marghany, A., & Abdelshafeek, K. A. (2020). Removal of Lead (II) from Synthetic Wastewater by Lavandula pubescens Decne Biosorbent: Insight into Composition–Adsorption Relationship. *Applied Sciences*, *10*(21), 7450.
4. Aziz, H. A., Adlan, M. N., Zahari, M. S. M., & Alias, S. (2004). Removal of ammoniacal nitrogen (N-NH3) from municipal solid waste leachate by using activated carbon and limestone. *Waste Management & Research*, *22*(5), 371–375.
5. Bel Hadjltaief, H., Omri, A., Ben Zina, M., Da Costa, P., & Galvez, M. E. (2015). Titanium dioxide supported on different porous materials as photocatalyst for the degradation of methyl green in wastewaters. *Advances in Materials Science and Engineering*, *2015*.
6. Bezerra, M. A., Santelli, R. E., Oliveira, E. P., Villar, L. S., & Escaleira, L. A. (2008). Response surface methodology (RSM) as a tool for optimization in analytical chemistry. *Talanta*, *76*(5), 965–977.
7. De Almeida, R., Porto, R. F., Hinojosa, M. A. G., Sanches, L. C. M., Monteiro, B. B., Conde, A. L. F. M., Costa, A. M., Quintaes, B. R., Bila, D. M., & Campos, J. C. (2022). Monitoring of experimental landfill cells with membrane concentrate infiltration: A systematic assessment of leachate quality and treatment performance. *Process Safety and Environmental Protection*, *168*, 1155–1165.

8. Detho, A., Daud, Z., Rosli, M. A., Ridzuan, M. B., Awang, H., Kamaruddin, M. A., Tajarudin, H. A., & Halim, A. A. (2021). COD and ammoniacal nitrogen reduction from stabilized landfill leachate using carbon mineral composite adsorbent. *Desalination and Water Treatment*, *210*, 143–151.
9. Faisal, A. A. H., Al-Wakel, S. F. A., Assi, H. A., Naji, L. A., & Naushad, Mu. (2020). Waterworks sludge-filter sand permeable reactive barrier for removal of toxic lead ions from contaminated groundwater. *Journal of Water Process Engineering*, *33*, 101112. https://doi.org/10.1016/j.jwpe.2019.101112
10. Ferraz, F. M., & Yuan, Q. (2020). Organic matter removal from landfill leachate by adsorption using spent coffee grounds activated carbon. *Sustainable Materials and Technologies*, *23*, e00141.
11. Freundlich, H. M. F. (1906). Over the adsorption in solution. *J. Phys. Chem*, *57*(385471), 1100–1107.
12. Ghaedi, M., Ghayedi, M., Kokhdan, S. N., Sahraei, R., & Daneshfar, A. (2013). Palladium, silver, and zinc oxide nanoparticles loaded on activated carbon as adsorbent for removal of bromophenol red from aqueous solution. *Journal of Industrial and Engineering Chemistry*, *19*(4), 1209–1217.
13. Gripa, E., Daflon, S. D. A., de Almeida, R., da Fonseca, F. V., & Campos, J. C. (2023). Landfill leachate treatment by high-pressure membranes and advanced oxidation techniques with a focus on ecotoxicity and by-products management: A review. *Process Safety and Environmental Protection*, *173*, 747–764. https://doi.org/10.1016/j.psep.2023.03.074
14. Hashemian, S., Salari, K., & Yazdi, Z. A. (2014). Preparation of activated carbon from agricultural wastes (almond shell and orange peel) for adsorption of 2-pic from aqueous solution. *Journal of Industrial and Engineering Chemistry*, *20*(4), 1892–1900. https://doi.org/10.1016/j.jiec.2013.09.009
15. Haslina, H., NorRuwaida, J., Dewika, M., Rashid, M., Khairunnisa, M. P., & Azmi, M. A. D. (2021). Landfill Leachate Treatment Methods and Its Potential for Ammonia Removal and Recovery-A Review. *IOP Conference Series: Materials Science and Engineering*, *1051*(1), 012064.
16. Hill, A. V. (1910). The possible effects of the aggregation of the molecules of haemoglobin on its dissociation curves. *J. Physiol.*, *40*, 4–7.
17. Ho, Y.-S., & McKay, G. (1999). Pseudo-second order model for sorption processes. *Process Biochemistry*, *34*(5), 451–465.
18. Hosseini, S. N., Borghei, S. M., Vossoughi, M., & Taghavinia, N. (2007). Immobilization of TiO2 on perlite granules for photocatalytic degradation of phenol. *Applied Catalysis B: Environmental*, *74*(1–2), 53–62.
19. Hu, L., Zeng, G., Chen, G., Dong, H., Liu, Y., Wan, J., Chen, A., Guo, Z., Yan, M., & Wu, H. (2016). Treatment of landfill leachate using immobilized Phanerochaete chrysosporium loaded with nitrogen-doped TiO2 nanoparticles. *Journal of Hazardous Materials*, *301*, 106–118.
20. Huong, P. T., Jitae, K., Giang, B. L., Nguyen, T. D., & Thang, P. Q. (2019). Novel lanthanum-modified activated carbon derived from pine cone biomass as ecofriendly bio-sorbent for removal of phosphate and nitrate in wastewater. *Rendiconti Lincei. Scienze Fisiche e Naturali*, *30*, 637–647.
21. Khan, A. R., Al-Waheab, I. R., & Al-Haddad, A. (1996). A generalized equation for adsorption isotherms for multi-component organic pollutants in dilute aqueous solution. *Environmental Technology*, *17*(1), 13–23.

22. Khan, A. R., Ataullah, R., & Al-Haddad, A. (1997). Equilibrium adsorption studies of some aromatic pollutants from dilute aqueous solutions on activated carbon at different temperatures. *Journal of Colloid and Interface Science*, *194*(1), 154–165.
23. Koble, R. A., & Corrigan, T. E. (1952). Adsorption isotherms for pure hydrocarbons. *Industrial & Engineering Chemistry*, *44*(2), 383–387.
24. Kumar, A., & Jena, H. M. (2015). High surface area microporous activated carbons prepared from Fox nut (Euryale ferox) shell by zinc chloride activation. *Applied Surface Science*, *356*, 753–761.
25. Lagergren, S. (1898). *Zur theorie der sogenannten adsorption geloster stoffe*.
26. Li, X., Liu, Y., Hao, J., & Wang, W. (2018). Study of almond shell characteristics. *Materials*, *11*(9), 1782.
27. Li, Z., Kechen, X., & Yongzhen, P. (2018). Composition characterization and transformation mechanism of refractory dissolved organic matter from an ANAMMOX reactor fed with mature landfill leachate. *Bioresource Technology*, *250*, 413–421.
28. Liu, J., Jiang, J., Meng, Y., Aihemaiti, A., Xu, Y., Xiang, H., Gao, Y., & Chen, X. (2020). Preparation, environmental application and prospect of biochar-supported metal nanoparticles: A review. *Journal of Hazardous Materials*, *388*, 122026.
29. Mosanefı, S., Alavi, N., Eslami, A., Saadani, M., & Ghavami, A. (2021). Ammonium removal from landfill fresh leachate using zeolite as adsorbent. *Journal of Material Cycles and Waste Management*, *23*, 1383–1393.
30. Naji, L. A., Faisal, A. A., Rashid, H. M., Naushad, M., & Ahamad, T. (2020). Environmental remediation of synthetic leachate produced from sanitary landfills using low-cost composite sorbent. *Environmental Technology & Innovation*, *18*, 100680.
31. Omri, A., & Benzina, M. (2019). Influence of the origin of carbon support on the structure and properties of TiO2 nanoparticles prepared by dip coating method. *Arabian Journal of Chemistry*, *12*(8), 2926–2936.
32. Peng, L., Qin, P., Lei, M., Zeng, Q., Song, H., Yang, J., Shao, J., Liao, B., & Gu, J. (2012). Modifying Fe3O4 nanoparticles with humic acid for removal of Rhodamine B in water. *Journal of Hazardous Materials*, *209*, 193–198.
33. Pipil, H., Yadav, S., Chawla, H., Taneja, S., Verma, M., Singla, N., & Haritash, A. K. (2022). Comparison of TiO2 catalysis and Fenton's treatment for rapid degradation of Remazol Red Dye in textile industry effluent. *Rendiconti Lincei. Scienze Fisiche e Naturali*, *33*(1), 105–114.
34. Prasad, R. K., & Srivastava, S. N. (2009). Sorption of distillery spent wash onto fly ash: Kinetics, mechanism, process design and factorial design. *Journal of Hazardous Materials*, *161*(2–3), 1313–1322.
35. Redlich, O., & Peterson, D. L. (1959). A useful adsorption isotherm. *Journal of Physical Chemistry*, *63*(6), 1024–1024.
36. Ringot, D., Lerzy, B., Chaplain, K., Bonhoure, J.-P., Auclair, E., & Larondelle, Y. (2007). In vitro biosorption of ochratoxin A on the yeast industry by-products: Comparison of isotherm models.

Bioresource Technology, *98*(9), 1812–1821. https://doi.org/10.1016/j.biortech.2006.06.015

37. Rodriguez-Narvaez, O. M., Peralta-Hernandez, J. M., Goonetilleke, A., & Bandala, E. R. (2019). Biochar-supported nanomaterials for environmental applications. *Journal of Industrial and Engineering Chemistry*, *78*, 21–33.
38. Saka, C., Teğin, İ., & Kahvecioğlu, K. (2023). Sulphur-doped carbon particles from almond shells as cheap adsorbent for efficient Cd(II) adsorption. *Diamond and Related Materials*, *131*, 109542. https://doi.org/10.1016/j.diamond.2022.109542
39. Shadi, A. M. H., Kamaruddin, M. A., Niza, N. M., Emmanuel, M. I., Hossain, M. S., & Ismail, N. (2020). Efficient treatment of raw leachate using magnetic ore iron oxide nanoparticles Fe□O□ as nanoadsorbents. *Journal of Water Process Engineering*, *38*, 101637.
40. Singh, K. (2021). Utilization of Nanoparticle-Loaded Adsorbable Materials for Leachate Treatment. *Nanobiotechnology for Green Environment*, 229–248.
41. Singh, K., Abdullahi, W. S., & Ram, C. (2018). Removal of heavy metals by adsorption using agricultural based residue: A review. *Res. J. Chem. Environ*, *22*(5), 65–74.
42. Singh, K., Lohchab, R. K., & Kumari, M. (2022). Impregnation of zinc oxide nanoparticles on activated carbon synthesised from corncob for appraisal of leachate chemical oxygen demand removal potential. *International Journal of Environmental Analytical Chemistry*, 1–24.
43. Singh, K., Lohchab, R. K., Kumari, M., & Beniwal, V. (2021). Potential of TiO2 loaded almond shell derived activated carbon for leachate treatment: Isotherms, kinetics, and Response Surface Methodology. *International Journal of Environmental Analytical Chemistry*, 1–22.
44. Song, K., Ren, X., Zhang, Q., Xu, L., & Liu, D. (2022). Electrochemical treatment for leachate membrane retentate: Performance comparison of electrochemical oxidation and electro-coagulation technology. *Chemosphere*, *303*, 134986.
45. Taha, A. A., Moustafa, A. H. E., Abdel-Rahman, H. H., & Abd El-Hameed, M. M. A. (2018). Comparative biosorption study of Hg (II) using raw and chemically activated almond shell. *Adsorption Science & Technology*, *36*(1–2), 521–548.
46. Thamilselvi, V., & Radha, K. V. (2017). Silver Nanoparticle loaded corncob adsorbent for effluent treatment. *Journal of Environmental Chemical Engineering*, *5*(2), 1843–1854. https://doi.org/10.1016/j.jece.2017.03.020
47. Toth, J. (1971). State equation of the solid-gas interface layers. *Acta Chim. Hung.*, *69*, 311–328.
48. Vijayaraghavan, K., Padmesh, T. V. N., Palanivelu, K., & Velan, M. (2006). Biosorption of nickel (II) ions onto Sargassum wightii: Application of two-parameter and three-parameter isotherm models. *Journal of Hazardous Materials*, *133*(1–3), 304–308.
49. Weber, W. J., & Morris, J. C. (1963). Kinetics of adsorption on carbon from solution. *Journal of the Sanitary Engineering Division*, *89*(2), 31–60.
50. Wu, Z., Cheng, Z., & Ma, W. (2012). Adsorption of Pb (II) from glucose solution on thiol-functionalized cellulosic biomass. *Bioresource Technology*, *104*, 807–809.

51. Yang, X., Arias, M. E., & Ergas, S. J. (2023). Hybrid constructed wetlands amended with zeolite/biochar for enhanced landfill leachate treatment. *Ecological Engineering*, *192*, 106990. https://doi.org/10.1016/j.ecoleng.2023.106990

Figures

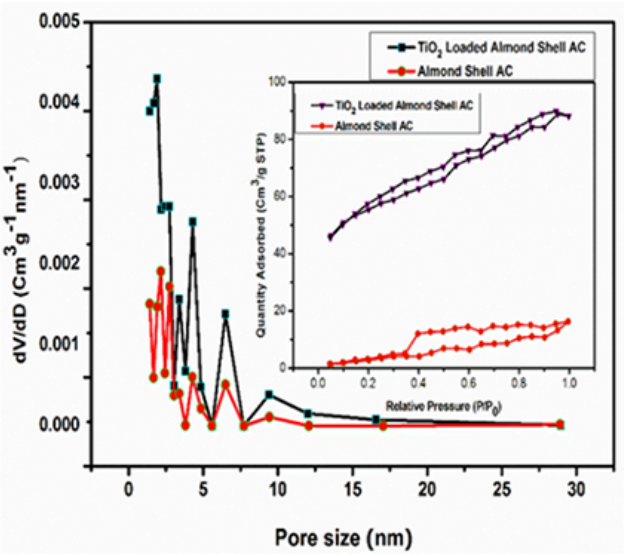

Figure 1(a).

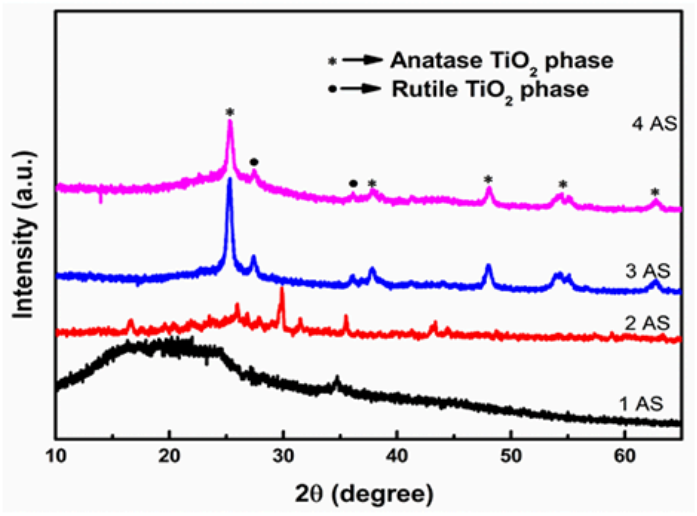

Figure 1(b).

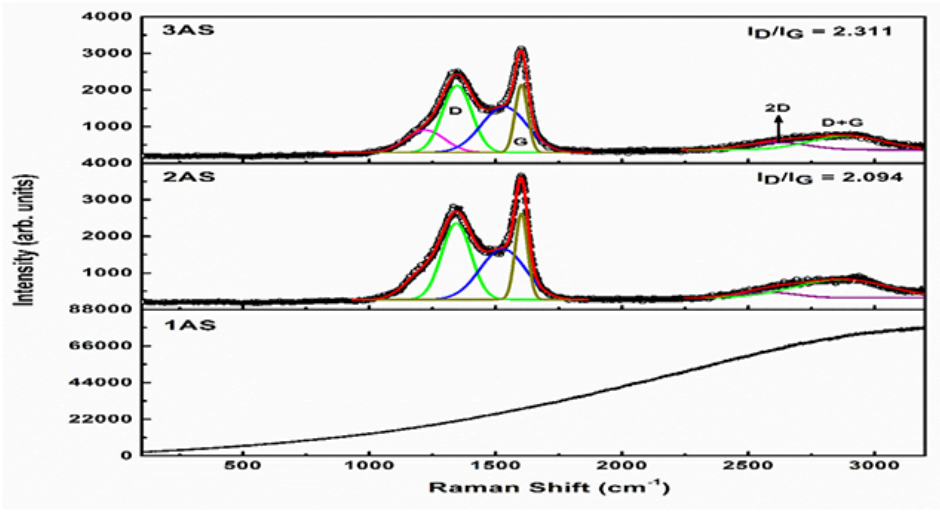

Figure 1(c).

Figure 1

(a). Sorption-desorption curve for N_2 and pore size distribution.

(b). The synthesised material's XRD pattern (Symbol * indicates the formation of both anatase and rutile TiO_2 phases). The sample symbols indicate 1AS as raw almond shell, 2AS as activated almond shell, 3AS as TiO_2 nanoparticle filled activated almond shell, and 4AS as TiO_2 nanoparticle loaded activated almond shell after treatment.

(c). Raman Spectra of AS, ASAc and TiO_2@ASAc

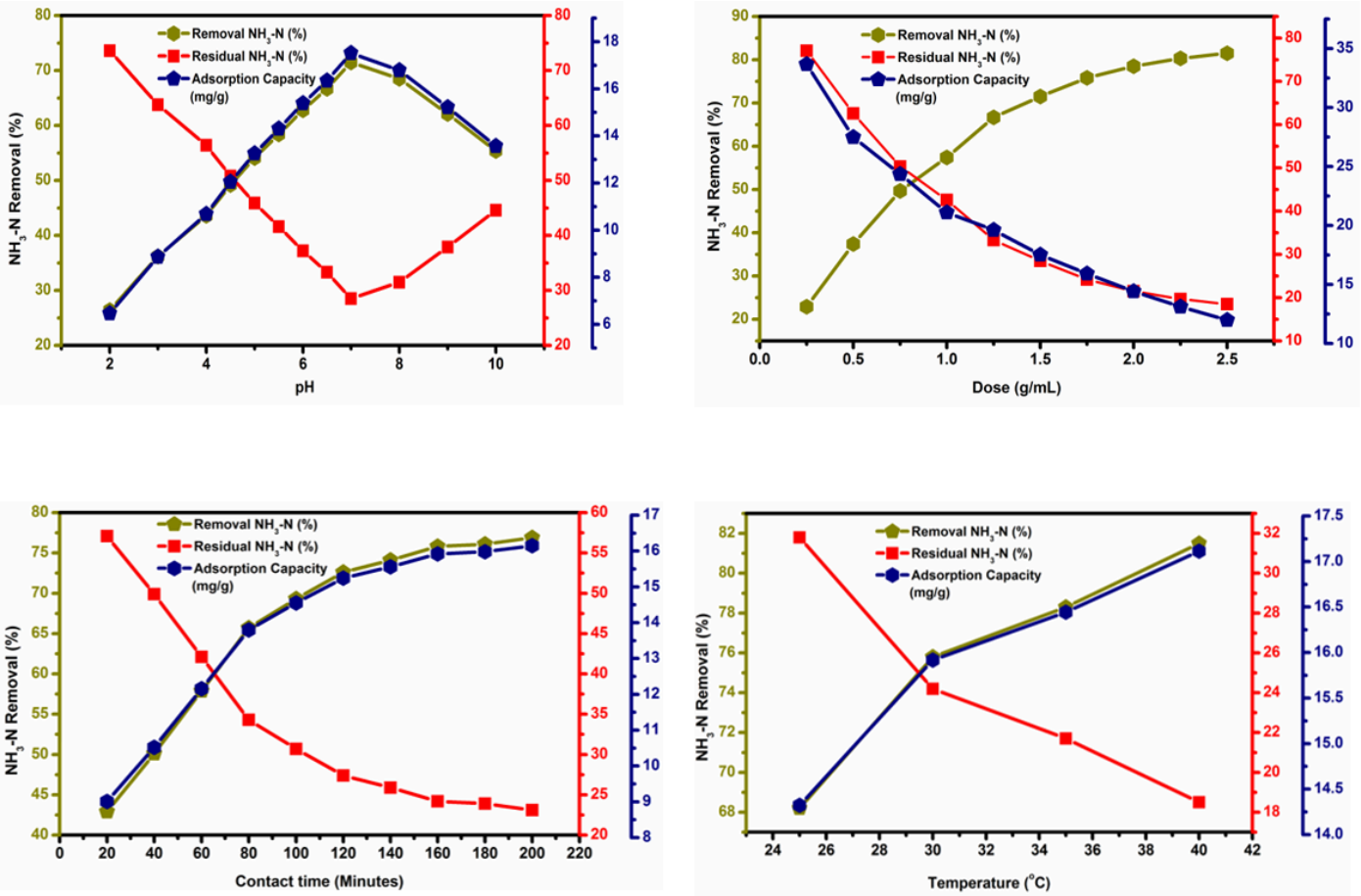

Figure 2

Influence of (a) pH, (b) dose, (c) contact time, and (d) temperature on NH_3-N removal

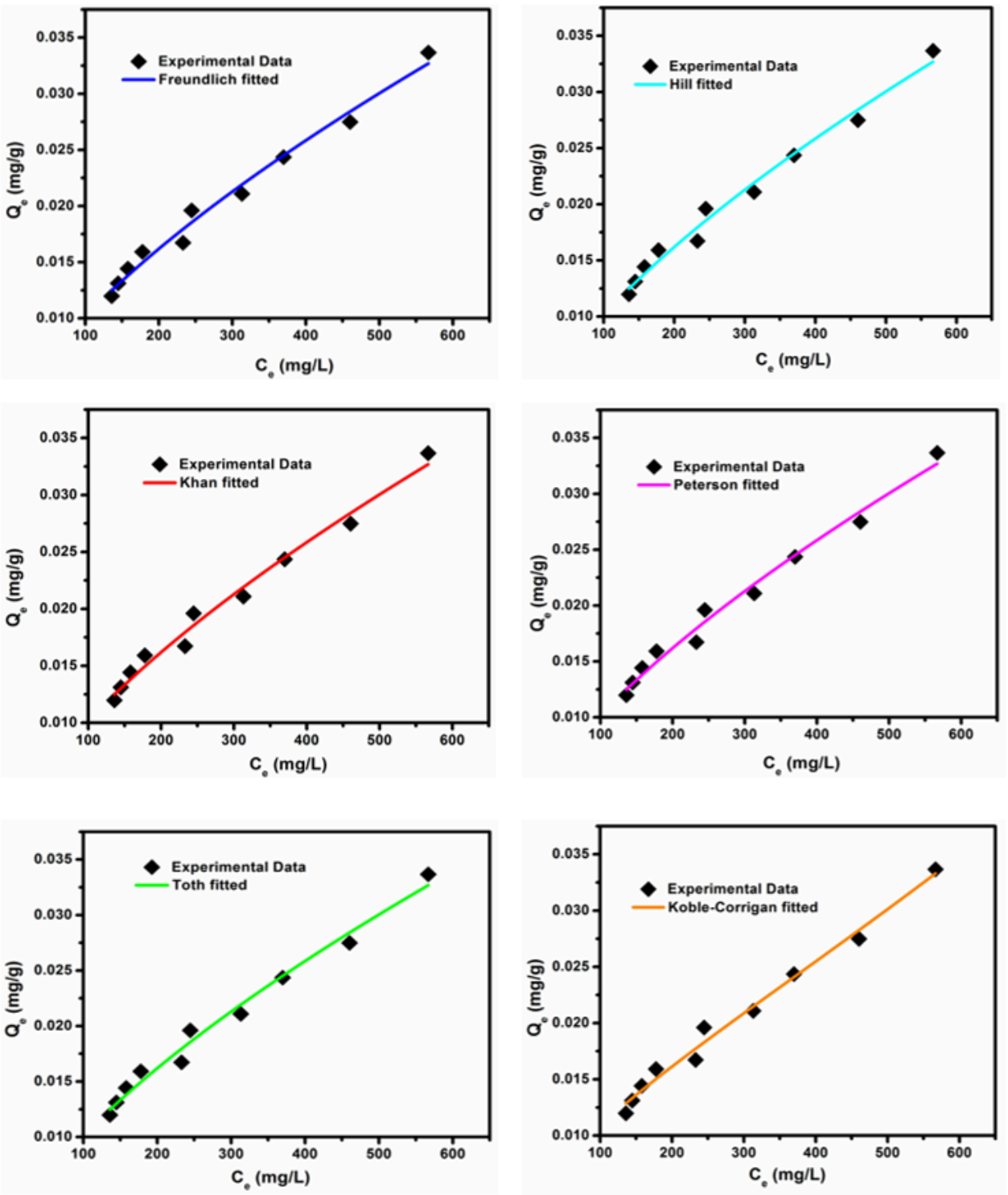

Figure 3

Isotherm studies for TiO_2@ASAc for NH_3-N removal

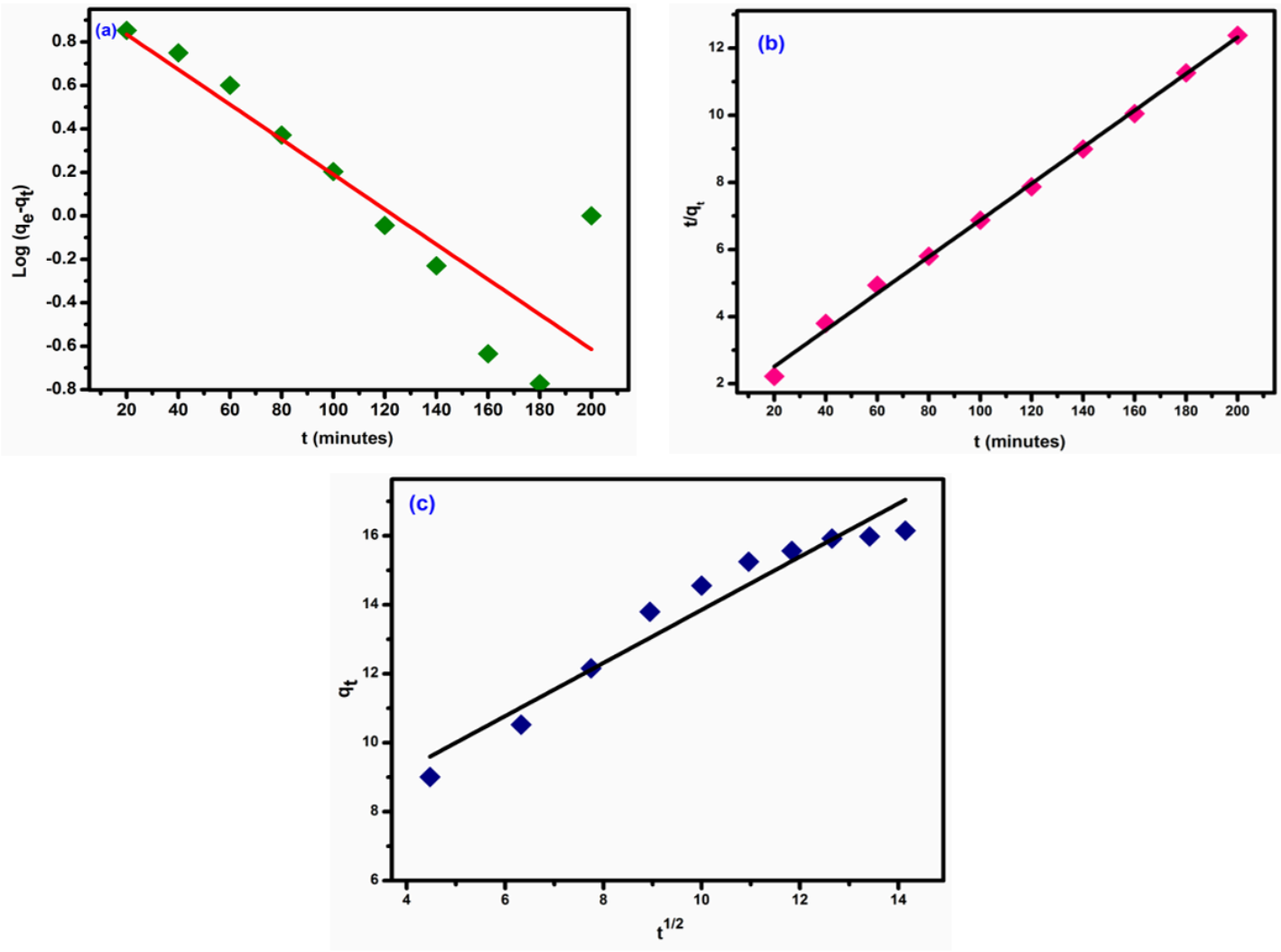

Figure 4

Plot of kinetic studies for NH_3-N removal by TiO_2@ASAc (a) Pseudo-first order, (b) Pseudo-second-order, and (c) Intraparticle diffusion.

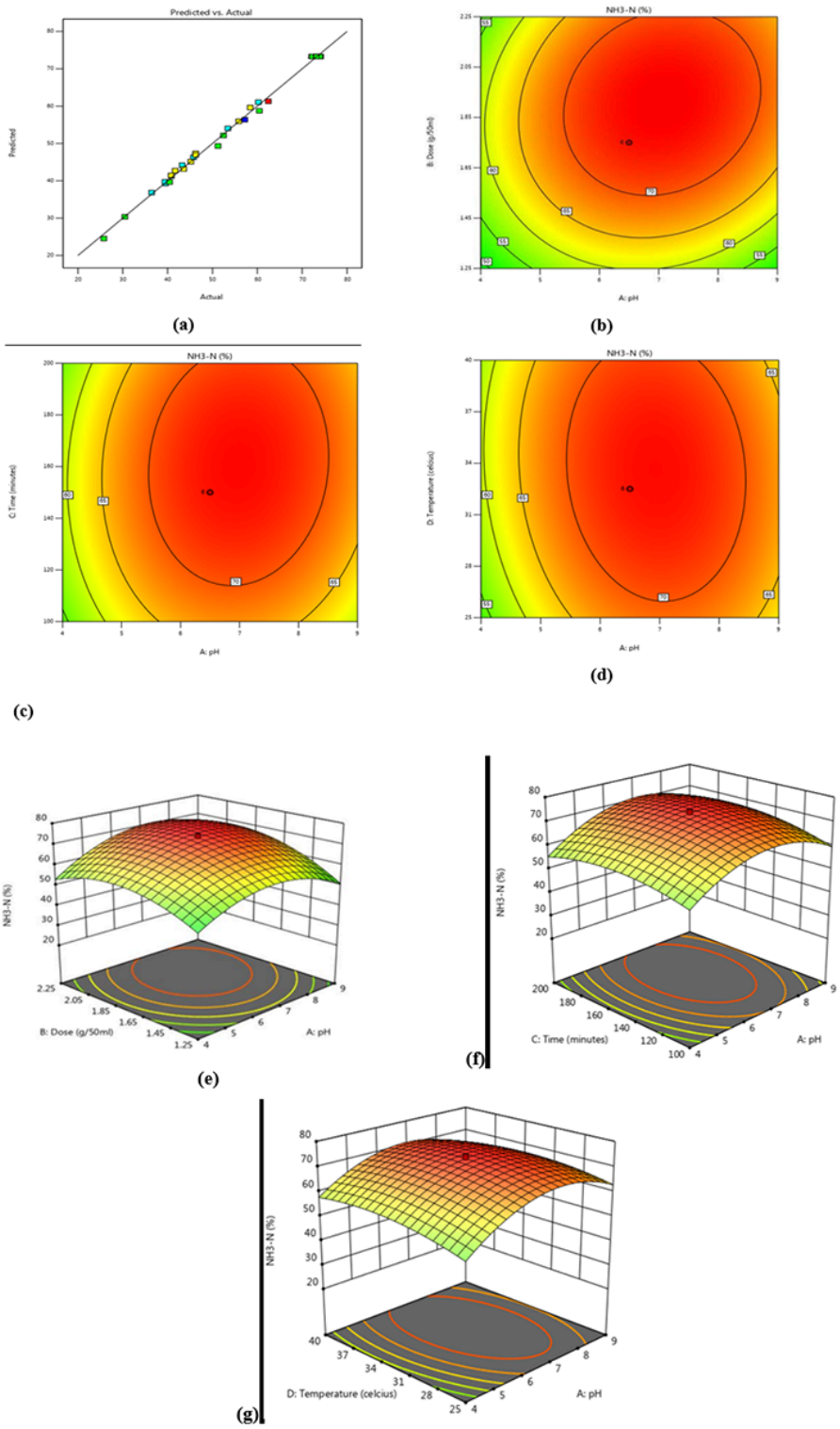

Figure 5

Predicted vs Actual and contour plots for NH_3-N removal (a-d), and 3D response plots for NH_3-N removal (e-g)

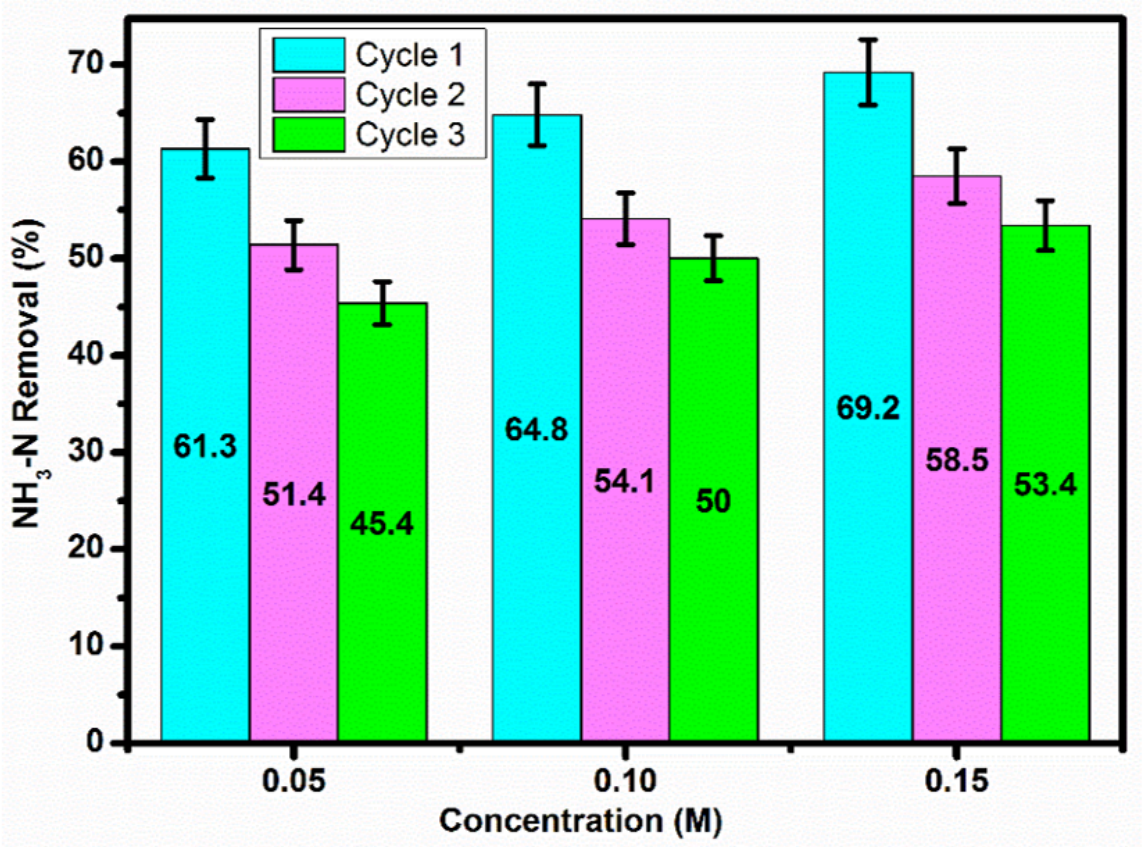

Figure 6

Efficiency of NH_3-N removal with regenerated TiO_2 nanoparticle loaded ASAc

Supplementary Files

This is a list of supplementary files associated with this preprint. Click to download.

- SupplimantryTables.docx